Impact of metal oxidation on ice growth and melting

S. Carretero-Palacios,[1,*] V. Esteso,[2,†] Y. Li,[3,4,‡] S. Kuthe,[5] I. Brevik,[6] K. Iordanidou,[7] O. I. Malyi,[8,9] B. Glaser,[5] C. Persson,[5,10,§] and M. Boström[9,11,‖]

[1]*Instituto de Ciencia de Materiales de Madrid, ICMM-CSIC, C/Sor Juana Inés de la Cruz, 3, 28049 Madrid, Spain*
[2]*Departamento de Física de la Materia Condensada, Instituto de Ciencia de los Materiales de Sevilla (ICMSE) – Consejo Superior de Investigaciones Científicas (CSIC), Universidad de Sevilla, P. O. Box 1065, Sevilla 41080, Spain*
[3]*Department of Physics, Nanchang University, Nanchang 330031, China*
[4]*Institute of Space Science and Technology, Nanchang University, Nanchang 330031, China*
[5]*Department of Materials Science and Engineering, KTH Royal Institute of Technology, SE-100 44 Stockholm, Sweden*
[6]*Department of Energy and Process Engineering, Norwegian University of Science and Technology, NO-7491 Trondheim, Norway*
[7]*Materials Physics-Oslo, SINTEF Industry, NO-0314 Oslo, Norway*
[8]*Qingyuan Innovation Laboratory, Quanzhou 362801, China*
[9]*Centre of Excellence ENSEMBLE3 Sp. z o. o., Wolczynska Str. 133, 01-919 Warsaw, Poland*
[10]*Centre for Materials Science and Nanotechnology, Department of Physics, University of Oslo, NO-0316 Oslo, Norway*
[11]*Chemical and Biological Systems Simulation Lab, Centre of New Technologies, University of Warsaw, Banacha 2C, 02-097 Warsaw, Poland*

(Received 10 September 2024; revised 20 December 2024; accepted 2 January 2025; published 7 February 2025; corrected 3 March 2026)

In this paper, we investigate the Casimir-Lifshitz free energy mechanism that governs both ice growth and melting near metal surfaces, with a particular focus on the role of oxidation. Our study reveals that metals such as gold, iron, and aluminum induce incomplete premelting, resulting in micron-sized liquid water layers when in contact with ice. These layers could have significant implications for the defrosting of metallic surfaces. When exposed to water vapor at the triple point, aluminum and other metals can induce the formation of notably thick layers of either liquid water or ice, which can theoretically become infinitely thick if other interactions are disregarded. However, when aluminum undergoes oxidation to form alumina, its behavior changes dramatically. Alumina surfaces cause complete melting when in direct contact with bulk ice and result in only micron-sized layers of water or ice in vapor conditions. In contrast, magnetite, the oxidized form of iron, retains metalliclike behavior due to its high dielectric constant, similar to other metals, and continues to support thick layers of water or ice. This distinction highlights the significant influence of oxidation on the dynamics of ice growth and melting near different metal surfaces.

DOI: 10.1103/PhysRevB.111.085407

I. INTRODUCTION

In 1991, Elbaum and Schick demonstrated a potential role for Casimir-Lifshitz interactions in the premelting of ice near the triple point of water [1]. In general, Casimir-Lifshitz [1,2] combined with double layer forces from impurity charges [2,3] can give rise to a short-range repulsion and long-range attraction in ice-water systems, which, in equilibrium, might result in the experimentally known partial ice premelting [4–6]. Such liquid water coatings created on ice surfaces [7–9] have been proposed to have a potential effect on the charging of thunderclouds [10–12], and on the rise of frost heave [13,14]. Recently, revised dielectric functions of water and ice [15–17] have resulted in new insights into the interaction of gas bubbles in organic liquid compounds [15], ice formation or melting in silver iodide with implications for cloud seeding and widespread rainfall [16], and potential effects on the insulation properties of ocean worlds against freezing through ice layer impacts on the buoyancy of CO_2 clathrate particles [18,19]. A proposal by Kobayashi *et al.* [20–22] suggests magnetically controlled heterogeneous ice nucleation in the presence of nanophase magnetite in supercooled water.

Here, we discuss a mechanism that may lead to ice growth and ice melting on metal surfaces. This is explored by employing the inhomogeneous Casimir-Lifshitz free energy theory we recently developed to study multilayer systems [23,24]. In the current case, it proves useful to study the simpler three-layer metal-water-ice and metal-ice-vapor systems, as schematically displayed in Fig. 1. We demonstrate how a metal in direct contact with a thick slab of ice causes its partial premelting, which induces a micron-sized liquid water layer at, or near, the triple point of water. The ability to induce partial premelting of ice on metallic surfaces opens avenues for designing antifreezing coatings crucial for aviation safety and infrastructure maintenance. Moreover, the control of ice nucleation by metallic particles holds promise for applications

*Contact author: sol.carretero@csic.es
†Contact author: vesteso@us.es
‡Contact author: leon@ncu.edu.cn
§Contact author: claspe@kth.se
‖Contact author: mathias.bostrom@ensemble3.eu

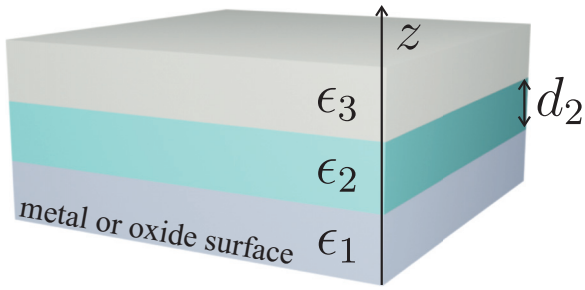

FIG. 1. Schematic figure of a three-layer system stacked along the z direction involved here: metal or oxide [aluminum (Al), alumina (Al_2O_3), gold (Au), iron (Fe), or magnetite (Fe_3O_4)] of infinite thickness and dielectric function ε_1, in contact with a layer of dielectric function ε_2, of thickness d_2, which is in turn in contact with a bulk material of dielectric function ε_3.

in weather modification and precipitation enhancement, while insights into the impact of metal oxidation on ice behavior are vital for improving material durability in harsh environments. By expanding the scope of ice studies to include metallic surfaces, this work broadens our understanding of ice behavior and paves the way for tailored solutions to diverse practical challenges. In what follows, we first describe the exploited material properties and present the theory used, and then, discuss our results ending with a brief summary.

II. MATERIAL PROPERTIES

The theory we will exploit is a direct extension of Casimir-Lifshitz dispersion force between interacting planar media originally derived by Lifshitz and coworkers [25]. In the early 1970s, Ninham and his team simplified the theoretical modeling of dispersion forces [26,27] and simultaneously extended it to account for magnetic effects [28]. However, the original Lifshitz theory was limited to dealing with only one layer extending to infinity. Recently, significant advancements have been made in expanding this theory to include two adjacent films, each capable of independently reaching infinite thickness. Esteso *et al.* [23] demonstrated this extension, followed by Luengo-Márquez and MacDowell [16]. Nevertheless, the consideration of such interactions in magnetodielectric materials has remained unexplored. In our current case, the magnetic contribution to the inhomogeneous Casimir-Lifshitz free energy is negligible, as we are using magnetite or nonmagnetic metals at one end of the structure. However, there are other systems, like magnetic fluids, where magnetic effects are known to be significant contributors [28–30]. These magnetic fluids could potentially offer intriguing possibilities for exploring magnetic interactions within the context of our expanded theory.

In order to investigate the Casimir-Lifshitz free energy or stress, we utilize the relative dielectric permittivity $\varepsilon(\omega) = \varepsilon'(\omega) + i\varepsilon''(\omega)$ of all materials, where $\varepsilon'(\omega)$ and $\varepsilon''(\omega)$ satisfy the Kramers-Kronig relation, and their corresponding values at discrete imaginary frequencies $\varepsilon(i\zeta_m)$ are exploited [31]. Here, $\zeta_m = m\zeta_T$, with $m = 0, 1, 2, ...,$ and $\zeta_T = 2\pi T$ represents the temperature-dependent frequency. In this expression, T denotes the temperature, and the remaining symbols are universal constants. Specifically, we consider a temperature of $T = 273.16$ K, which corresponds to the triple point of water for the systems under study. Both dielectric magnitudes at real and imaginary frequencies are related through Wick rotation: [31]

$$\varepsilon_j(i\zeta_m) = 1 + \frac{2}{\pi}\int_0^\infty d\omega \frac{\omega\varepsilon_j''(\omega)}{\omega^2 + \zeta_m^2} \tag{1}$$

with $j = 1$, 2, or 3, accounting for each material in the three-layer system.

The metals and oxides examined in this study, i.e., gold (Au), aluminum (Al), alumina (Al_2O_3), iron (Fe), and magnetite (Fe_3O_4), are cubic materials with a high degree of spatial isotropy, which minimizes the influence of surface orientation on their bulk dielectric properties. Similarly, the dielectric functions of Al_2O_3 and Fe_3O_4 exhibit minimal anisotropy for the Matsubara frequencies $m > 0$, supporting the macroscopic approach employed here. This framework assumes an averaged dielectric response and does not explicitly incorporate specific surface orientations or interfacial atomistic relaxations. While minor variations in surface properties, such as surface tension or stability, may arise due to orientation effects, they are generally modest for cubic systems. The methodology adopted is therefore well-suited to capturing the principal trends in Casimir-Lifshitz interactions for these materials. The dielectric permittivity $\varepsilon(\omega)$ for the materials here employed, are determined using the Kohn-Sham equation within the framework of the density functional theory (DFT), employing the projector augmented wave approach in the Vienna *Ab initio* Simulation Package [32,33].

In this study, we employed the generalized gradient approximation Perdew-Burke-Ernzerhof (PBEsol) [34] with Hubbard corrections on the d orbitals according to Dudarev *et al.* [35] to model the dielectric properties of the materials. Our calculations focus on bulk dielectric functions, where van der Waals (vdW) interactions are not the dominant forces and are therefore not explicitly included. While vdW corrections are crucial for systems dominated by noncovalent interactions, the materials studied here—metals and oxides—are not vdW-bound systems. The excellent agreement between our calculated dielectric constants and experimentally measured values validates the robustness of our approach without the need for additional vdW corrections. The energy cutoff was 400 eV; we use $U = 3.0$ eV for Au, $U = 2.0$ eV for bcc Fe, and $U = 5.7$ eV for Fe atoms in magnetite. This somewhat large Coulomb correction for Fe is needed when we include the eight semicore electrons in the electron density, while the interaction could be about 1 eV smaller if we would consider only the valence electrons. For metallic gold, iron, and aluminum with 1 atom per primitive cell, the k-space summation involved an $80 \times 80 \times 80$ k mesh and a Gaussian smearing of 0.05 eV. The resulting permittivity for gold and aluminum agrees with the experimental data presented in Ref. [36].

Regarding the magnetite, we consider the inverse spinel structure, stable above the Verwey transition temperature of about 120 K, and our analysis confirms the experimental findings [37–39] that the Fermi level is located in a narrow energy gap region. For this semiconducting phase with 14 atoms per primitive cell, we utilized the tetrahedron integration

TABLE I. Parametrization of the average dielectric function of continuous media, $\varepsilon(i\xi)$, at imaginary frequencies for Al, Fe_3O_4, and Fe as calculated with first-principles calculations as described in the text.

	Al		Fe_3O_4		Fe	
t	ω_t (eV)	c_t	ω_t (eV)	c_t	ω_t (eV)	c_t
1	0.0496	26141.8187	0.0209	49.338	0.0097	3.9659
2	0.0503	35471.2573	0.0772	7.7867	0.05	22634.316
3	0.27	26.8726	0.3127	4.7422	0.1012	15.5894
4	0.5495	30.0875	0.6912	3.6331	0.4368	3.6034
5	1.4796	14.4922	2.4508	1.2529	1.3519	8.8565
6	2.8411	2.8957	5.3771	2.2625	3.1276	8.9121
7	7.4905	0.1576	13.0017	1.1828	8.6427	2.0071
8	26.2452	0.0052	30.7646	0.3136	24.6372	0.5258
9	58.28387	0.003	72.2563	0.0672	75.3222	0.1035

over a $20 \times 20 \times 20$ k mesh. Draine and Hensley [40] have parametrized the dielectric permittivity of magnetite based on several published experimental data. Our calculated spectrum of $\varepsilon''(\omega)$ agrees overall very well with the measurements in the high infrared and the visible regions. Moreover, the ionic contribution in the low infrared region due to optical vibration modes matches also the experimental spectrum. However, the measurements indicate a rather strong and broad dielectric response around 0.4 eV, which is not consistent with the computed spectrum for the ideal magnetite. This may indicate the presence of a secondary phase in the material. Since we expect that our atomistic modeling accurately describes the response for frequencies higher than about 1 eV, while Draine and Hensley's adopted spectrum better describes a realistic material structure below 1 eV, we combine those two spectra. Then we also include the empirical model that accounts for the electrical conductivity at room temperature [40] yielding a metallic character of the low-frequency permittivity.

The crystalline structure of alumina is the well-known trigonal symmetry, space group $R\bar{3}c$, with a rhombohedral Bravais lattice with ten atoms per unit cell. The lattice parameters were determined in Ref. [41], and the dielectric functions were generated with a tetrahedron integration over a $12 \times 12 \times 12$ k mesh. Since alumina is a polar insulator, an electrical conductivity does not contribute at low frequencies, and instead, the dielectric response originates from the electronic interband transitions on the eV scale, combined with optical modes of vibrations on the 0.1-eV scale. We use the parameterized dielectric function at imaginary frequencies for alumina given in the literature [41]. To use the DFT calculated dielectric functions for Casimir-Lifshitz interaction, we develop a parametrization of the average dielectric function for each of the considered materials using an oscillator model:

$$\varepsilon(i\zeta_m) = 1 + \sum_t \frac{c_t}{1 + (\zeta_m/\omega_t)^2}. \tag{2}$$

Here, ω_t and c_t represent the characteristic frequencies and the oscillator strength, respectively. The parameters for Al, Fe_3O_4, and Fe are provided in Table I. The dielectric function for Au and Al_2O_3 were presented in a recent work [42]. For cases not considered here, where the low-frequency Drude/plasma modeling is important [43] (e.g., metal-media-metal), special treatment of the zero frequency contribution is essential.

The dielectric function for ice-cold water was recently reinvestigated by Fiedler *et al.* [15] and exploited for astrophysical applications [18]. We use in the current work dielectric functions for ice and water within similarly improved parametrizations [16,17]. In this study, water is modeled as a dielectric medium, treated as an insulator to simplify the calculations of Casimir-Lifshitz forces. Under realistic conditions, however, water behaves as an electrolyte due to the presence of ions such as H^+ and OH^-, with a Debye length at room temperature of approximately 1000 nm in the absence of air, or around 220 nm when exposed to air, as dissolved CO_2 increases ion concentration in the water [44,45]. This introduces the potential for ionic-charge fluctuations to influence interfacial properties, especially at distances comparable to or exceeding the Debye length. These considerations, though beyond the current scope, highlight important factors to be addressed in future refinements of this model. The dielectric functions $\varepsilon(i\zeta_m)$ for Au, Al, Al_2O_3, Fe, and Fe_3O_4, water (H_2O) [16,17], and ice (H_2O(s)) [16,17] are shown in Fig. 2.

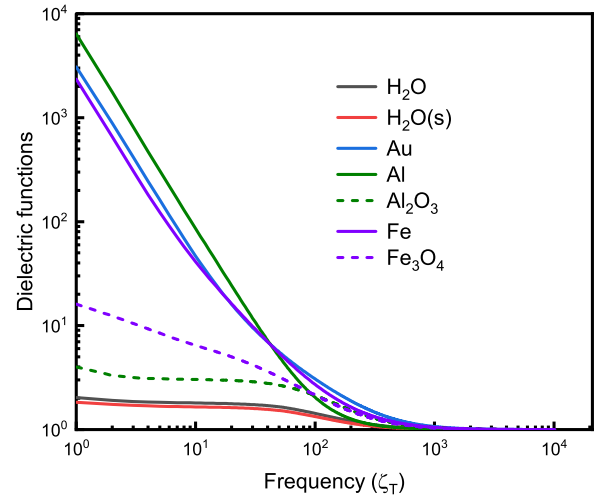

FIG. 2. Dielectric function evaluated at the imaginary frequencies, $\varepsilon(i\zeta)$, for water (H_2O) [16,17], ice (H_2O(s)) [16,17], Au, Al, Al_2O_3, Fe, and Fe_3O_4, with their static values ($\varepsilon(0)$) being 88.2, 91.5, 3.70×10^4, 5.67×10^4, 10.1, 2.09×10^4, and 54.8, accordingly. The imaginary frequency is normalized in units of ζ_T at $T = 273.16$ K.

Very similar results would be obtained if an alternative set of dielectric functions for ice [1] and water [15] were used. One should perhaps mention that the parameterized models for ice and water by Luengo-Márquez and MacDowell [17] agree very well (except at very low frequencies) with the dielectric functions for imaginary frequencies derived from experimental data on the real frequency axis, but they do not obey the Kramers-Kronig relation (causality) which is valid for the model by Fiedler, Parsons, and coworkers [15]. Therefore when using the Luengo-Márquez and MacDowell model, one must insert the zero frequency dielectric constant separately.

III. THEORY

In this paper, natural units $\hbar = c = \varepsilon_0 = \mu_0 = k_B = 1$ are used, unless explicitly specified. The Casimir-Lifshitz free energy per unit area for a three-layer system is [25,28,43]

$$F = \frac{T}{2}\sum_{m=-\infty}^{\infty}\int\frac{d^2k}{(2\pi)^2}\sum_{\sigma=\mathrm{E,H}}\ln\left(1-r_{12}^{\sigma}r_{32}^{\sigma}e^{-2\kappa_2 d_2}\right), \quad (3)$$

where the Fresnel reflection coefficients for transverse electric ($\sigma = \mathrm{E}$) and transverse magnetic ($\sigma = \mathrm{H}$) waves are given as [28]

$$r_{np}^{\mathrm{E}} = \frac{\mu_p\kappa_n^{\perp} - \mu_n\kappa_p^{\perp}}{\mu_p\kappa_n^{\perp} + \mu_n\kappa_p^{\perp}}, \quad r_{np}^{\mathrm{H}} = \frac{\varepsilon_p\kappa_n^{\perp} - \varepsilon_n\kappa_p^{\perp}}{\varepsilon_p\kappa_n^{\perp} + \varepsilon_n\kappa_p^{\perp}}. \quad (4)$$

with subscripts n and p indicating two adjacent materials. In these expressions, electromagnetic response properties of the medium j are described by its permittivity ε_j and permeability μ_j, and the perpendicular wave vector [28] here is expressed as $\kappa_n^{\perp} = \sqrt{k^2 + \mu_n(i\zeta_m)\varepsilon_n(i\zeta_m)\zeta_m^2}$. The corresponding Hamaker constant is [46]

$$A_{123} = -6T\sum_{m=0}^{\infty}{}'\int_0^{\infty} dqq\ln\left[1 - \frac{(\varepsilon_1-\varepsilon_2)(\varepsilon_3-\varepsilon_2)}{(\varepsilon_1+\varepsilon_2)(\varepsilon_3+\varepsilon_2)}e^{-2q}\right], \quad (5)$$

where the sum is done over discrete Matsubara frequencies defined above, and the prime in the summation indicates that the $m = 0$ term should be divided by a factor two.

To investigate the growth or melting of ice near metallic surfaces triggered by the fluctuating electromagnetic field, we leverage the data previously discussed in this section pertaining to the permittivity of each material across a range of Matsubara frequencies. In the scenarios examined in this study, the zero-frequency limit of the reflection coefficient, denoted as r_{np}^{H}, exhibits minimal sensitivity to the treatment of low-frequency metallic permittivities. However, in alternate scenarios such as metal-air-metal configurations, it has been demonstrated that outcomes are significantly influenced by the behavior of permittivity at low frequencies [43,47]. Most materials here are essentially nonmagnetic, with the permeability nicely approximated as $\mu_n(i\zeta_m) = 1$. The magnetic susceptibility for magnetite is given by Velchiko *et al.* [30] and by Draine and Hensley [40]. However, since the permeability is extremely close to one for nonzero Matsubara frequencies [30], and the relevant combinations of reflection coefficients always lead to zero-frequency contributions independent of permeabilities, the magnetic corrections from the magnetite are in our case unimportant for the Casimir-Lifshitz free energy. For example, with the magnetite included, the nonzero r_{12}^{E} term for zero frequency is always multiplied by vanishing terms, as shown in Eq. (3). At short separation distances, when the finite velocity of light can be considered "infinite", the product of reflection coefficients in the expression for the free energy is proportional to

$$\frac{(\varepsilon_1-\varepsilon_2)(\varepsilon_3-\varepsilon_2)}{(\varepsilon_1+\varepsilon_2)(\varepsilon_3+\varepsilon_2)}. \quad (6)$$

This expression, evaluated at Matsubara frequencies, indicates that certain frequency ranges (e.g., at zero frequency) with dielectric functions satisfying $\varepsilon_1(i\zeta_m) > \varepsilon_2(i\zeta_m) > \varepsilon_3(i\zeta_m)$ can lead to a repulsive interaction. In contrast, for cases where the product is positive, an attractive interaction can result.

IV. RESULTS

To explore the influence of Casimir-Lifshitz interactions on the growth or melting of ice near metallic surfaces, our analysis focuses on a three-layer system denoted as ε_1-ε_2-ε_3. We investigate both the nonretarded and retarded regimes of these interactions. In the non-retarded limit, where the separations are small enough that the speed of light can be considered infinite in the free energy expression, the interactions can be described using Hamaker constants [46]. The Hamaker constant A_{123} for the system is given by $A_{123} = -12\pi d_2^2 F(d_2)$, where d_2 represents the thickness of the intervening medium (ε_2). Additionally, we consider the contribution from the $m = 0$ term alone, denoted $A_{123;0}$. The sign of these constants indicates the nature of the interaction: positive A_{123} indicates short-range attraction; positive $A_{123;0}$ indicates long-range attraction; and negative A_{123} or $A_{123;0}$ indicates repulsion. When both A_{123} and $A_{123;0}$ are negative, the thickness d_2 of the intervening layer increases infinitely, leading to the complete separation of layers by a thick medium. Conversely, if A_{123} is negative (indicating repulsion) but $A_{123;0}$ is positive (indicating attraction), a finite d_2 layer forms, leading to partial melting.

In the retarded regime, as the thickness d_2 of the intervening layer increases, the finite speed of light must be taken. In this regime, the interaction diminishes more rapidly with increasing d_2, specifically as $\propto 1/d_2^3$, compared to the nonretarded regime. For larger thicknesses, the interaction energy becomes predominantly influenced by the purely entropic contribution associated with the $m = 0$ term, causing the long-range interaction to be dominated by $A_{123;0}$.

Understanding the interplay between A_{123} and $A_{123;0}$ provides insights into the behavior of ice growth and melting. This relationship is critical in explaining phenomena such as the transition from partial to complete melting when a metal layer undergoes oxidation. These relationships are summarized in Table II, which illustrates how different combinations of A_{123} and $A_{123;0}$ affect the behavior of the intervening layer (ε_2) and the overall system. As shown in Table II, the calculated equilibrium thickness (if any), d_2^{eq}, at which a free energy minimum occurs, are comparable to or larger than the Debye length of water at room temperature. This suggests that ionic-charge fluctuations, which are not considered here, may significantly influence the Casimir-Lifshitz interactions,

TABLE II. The Hamaker constant [46] A_{123} and its contributions from the zeroth Matsubara term $A_{123;0}$ for various three-layer configurations at T=273.16 K. In the last column the equilibrium thickness (if any), d_2^{eq}, is given. This thickness corresponds to the value which leads to a free energy minimum.

Configurations (1-2-3)	A_{123} (meV)	$A_{123;0}$ (meV)	d_2^{eq} (nm)
Water-ice-vapor	-4.74×10^{1}	3.18×10^{-1}	1043.6
Au-water-vapor	-7.62×10^{2}	-1.55×10^{1}	∞
Au-ice-vapor	-6.56×10^{2}	-1.55×10^{1}	∞
Fe-water-vapor	-6.88×10^{2}	-1.55×10^{1}	∞
Fe-ice-vapor	-6.02×10^{2}	-1.55×10^{1}	∞
Fe_3O_4-water-vapor	-4.24×10^{2}	4.15×10^{0}	1234.4
Fe_3O_4-ice-vapor	-3.88×10^{2}	4.47×10^{0}	1163.9
Al-water-vapor	-5.45×10^{2}	-1.55×10^{1}	∞
Al-ice-vapor	-4.97×10^{2}	-1.56×10^{1}	∞
Al_2O_3-water-vapor	-3.06×10^{2}	1.55×10^{1}	196.4
Al_2O_3-ice-vapor	-2.87×10^{2}	1.57×10^{1}	201.3
Au-water-ice	-1.46×10^{2}	3.23×10^{-1}	2080.2
Fe-water-ice	-1.27×10^{2}	3.22×10^{-1}	2078.0
Fe_3O_4-water-ice	-8.13×10^{1}	-7.56×10^{-2}	∞
Al-water-ice	-8.87×10^{1}	3.24×10^{-1}	2089.2
Al_2O_3-water-ice	-6.60×10^{1}	-2.57×10^{-1}	∞
Au-ice-water	1.57×10^{2}	-3.22×10^{-1}	$0/\infty$
Al-ice-water	9.89×10^{1}	-3.22×10^{-1}	$0/\infty$
Al_2O_3-ice-water	7.83×10^{1}	2.60×10^{-1}	0
Fe-ice-water	1.73×10^{2}	-3.21×10^{-1}	$0/\infty$
Fe_3O_4-ice-water	9.32×10^{1}	8.13×10^{-2}	0

particularly the contribution from the first Matsubara term ($m = 0$). Recent studies [48–51] provide insights into how these effects could be incorporated in future work.

Aluminum is a particularly interesting case. As a highly reactive material, it readily forms an oxide layer (alumina) several nanometers thick when exposed to air. This alumina layer significantly modifies the Casimir-Lifshitz interactions at the interface, resulting in distinct ice growth and melting behaviors compared to either unoxidized aluminum or fully oxidized alumina. Specifically, oxidation transforms aluminum's partial premelting behavior into the complete melting behavior characteristic of alumina. While our study focuses on the idealized cases of fully unoxidized or fully oxidized aluminum, intermediate scenarios involving finite-sized oxidation layers could exhibit unique properties. Investigating these effects, analogous to finite-size low-occupancy gas hydrate layers studied in hydrate-water interfaces [18], would provide additional insights. In the case of aluminum, the transition from nonoxidized to fully oxidized states demonstrates how surface oxidation impacts ice-melting dynamics. This relationship underscores the importance of understanding oxidation and layer thickness in determining ice behavior. By situating these findings within the Casimir-Lifshitz framework, we offer a comprehensive explanation of how material-specific properties and oxidation states govern ice growth and melting processes. This framework of Casimir-Lifshitz interactions and their impact on ice growth and melting provides a comprehensive understanding of the influence of metal oxidation states and layer thickness on these processes.

To analyze the results in Figs. 3 and 4, we consider medium ε_1 as being in contact with medium ε_3 through medium ε_2. Here we consider medium ε_2 to be either water or ice depending on the thermodynamic initial conditions. We examine the behavior of the layer thickness of medium ε_2, which can stabilize at a finite size, disappear, or grow infinitely. These scenarios correspond to different behaviors of the Casimir-Lifshitz free energy curves. In the stabilization scenario, the Casimir-Lifshitz free energy initially decreases (short-range repulsive interaction) and then increases (long-range attractive interaction), creating a minimum in the free energy and leading to the formation of a stable thin layer of medium ε_2. In the disappearance scenario, the free energy curve increases monotonically with increasing thickness, resulting in attractive Casimir-Lifshitz forces that cause medium ε_2 to vanish. Finally, in the infinite growth scenario, the free energy curve decreases monotonically with increasing thickness of medium ε_2, leading to repulsive Casimir-Lifshitz forces that cause the intervening medium to continually grow.

Figure 3 shows the full calculation of the Casimir-Lifshitz free energies per unit area when retarded effects are taken into account [employing Eq. (3)] for various three-layer systems involving aluminum (a) or alumina (b) in contact with water-ice (blue), ice-water (green), water-vapor (black), and ice-vapor (dashed red line). In Fig. 3(a), for the aluminum-water-ice system, a stable water layer approximately 2 μm thick is formed, as indicated by a minimum in the free energy, signifying incomplete surface freezing of ice. In the aluminum-ice-water system, the intervening ice layer is suppressed, as shown by the monotonous increase in free energy as a function of d_2. In the aluminum-water-vapor system, the intervening water layer forms under moist conditions. Finally, for the aluminum-ice-vapor system, depending on initial conditions, the system can similarly foster the growth of infinitely thick ice layers on the metal surface. When aluminum undergoes severe oxidation, forming a bulk alumina layer [Fig. 3(b)], distinct behaviors are observed. In alumina-water-ice (blue curve) and alumina-ice-water (green curve) systems, complete melting occurs due to forces of differing signs. Specifically, oxidation in an ice-water system (green curve) does not result in any change, but in a water-ice interface (blue curve), it leads to the elimination of the finite water layer present without oxidation. Additionally, when alumina is exposed to vapor instead of ice, it causes the formation of ice (red curve) or water (black curve) layers, each hundreds of nanometers thick, on the alumina surface. This contrasts with the infinite growth observed in the absence of oxidation (a). Similar trends are predicted for iron in Fig. 4(a) versus magnetite, in Fig. 4(b), as expected according to the results in Table II. Here, equilibrium distances occur at greater thicknesses for the oxidized form of Fe compared to Al due to the higher dielectric constant of Fe_3O_4. Thus, the presence of a thick oxidation layer significantly influences the dynamics of ice growth and melting when in contact with metals.

V. SUMMARY AND CONCLUSIONS

Micron-sized premelting layers, or thicker, often manifest near specific ice interfaces. A straightforward assumption

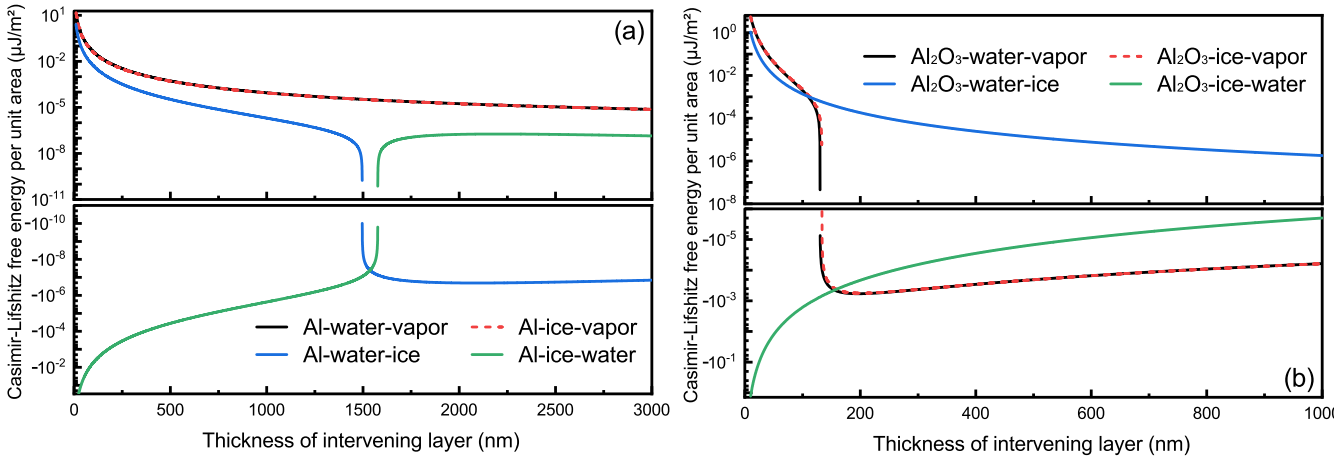

FIG. 3. The Casimir-Lifshitz free energy ($T = 273.16$ K), as a function of the thickness of the intervening layer, calculated for different configurations: (a) Al-water-ice, Al-ice-water, Al-water-vapor, and Al-ice-vapor, and (b) Al_2O_3-water-ice, Al_2O_3-ice-water, Al_2O_3-water-vapor, and Al_2O_3-ice-vapor. In both panels, the last two cases virtually overlap on the scale shown.

might be that, under identical temperature conditions (such as the triple point of water) and with the same materials (e.g., aluminum, gold, iron, magnetite, or alumina), we would observe either ice melting or ice formation, but not both simultaneously. However, as highlighted by Wilen *et al.* [2], the choice of material combinations can significantly influence the resulting outcomes. Here, we investigated the Casimir-Lifshitz free energy mechanisms driving the growth and melting of ice near metallic surfaces, emphasizing the crucial role of oxidation. Our analysis, focused on a three-layer system, reveals several significant findings.

On the one hand, we find that the strong oxidation of metals such as aluminum and iron, when in contact with an ice-water interface, does not alter the interaction compared to non-oxidized scenarios. This means that the presence or absence of a thick oxide layer does not significantly change the dynamics of the system in the ice-water context. Contrarily, in water-ice systems, the presence of a robust oxidation layer on aluminum or iron induces a dramatic shift in behavior. The oxidation leads to complete melting, thus eliminating the finite water layer that exists when the metals are not oxidized. This transition underscores the sensitivity of the water-ice interface to the oxidation state of the metals, where the dielectric properties of the materials play a pivotal role in determining the system's behavior.

In vapor conditions, particularly at the triple point of water, the oxidation state again proves critical. Strongly oxidized metals foster the formation of finite, stable layers of either water or ice on their surfaces. This is in stark contrast to the unbounded growth of these layers in non-oxidized systems, where infinite thickness is theoretically possible. This finding illustrates how oxidation imposes constraints on layer thickness, fundamentally altering the growth dynamics in vapor.

Additionally, our results have broader implications for metal surfaces exposed to water vapor at the triple point. Metals such as gold, iron, magnetite, and aluminum can

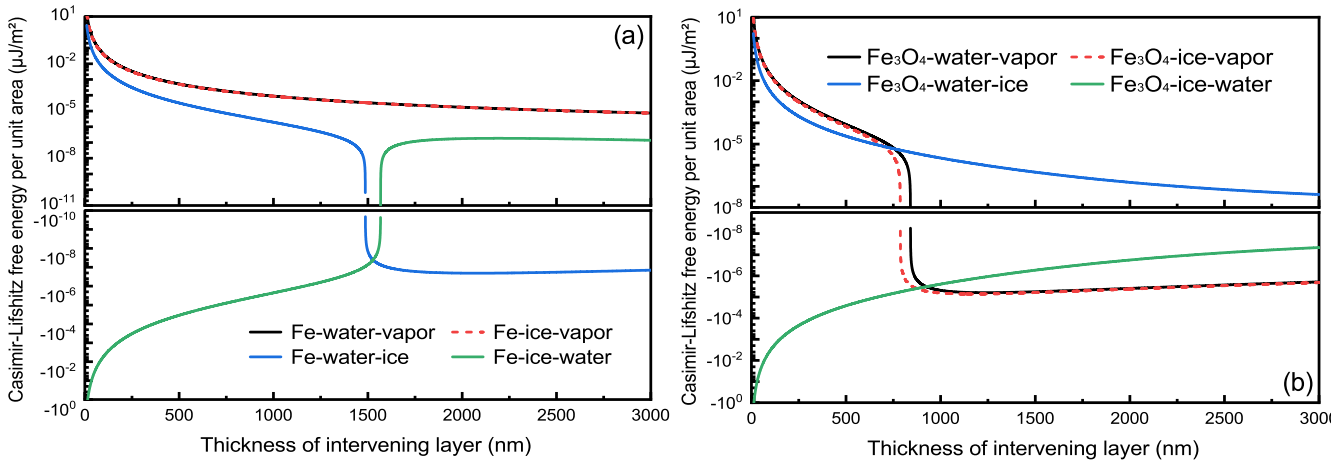

FIG. 4. The Casimir-Lifshitz free energy ($T = 273.16$ K), as a function of the thickness of the intervening layer, calculated for different configurations: (a) Fe-water-ice, Fe-ice-water, Fe-water-vapor, and Fe-ice-vapor, and (b) Fe_3O_4-water-ice, Fe_3O_4-ice-water, Fe_3O_4-water-vapor, and Fe_3O_4-ice-vapor. In panel (a), the last two cases virtually overlap on the scale shown.

induce either infinite layers of liquid water or ice, depending on initial conditions and surface properties. This suggests that the behavior of these systems is highly dependent on the initial setup and the specific interactions between the metal and the water molecules.

These findings hold significant implications for understanding the complex interplay between material properties, environmental conditions, and phase transitions at solid-liquid interfaces. Understanding the nuanced behavior of different materials in contact with ice, particularly in the presence of varying environmental factors such as humidity and chemical composition, is crucial for numerous applications ranging from cryopreservation and ice adhesion mitigation to climate modeling and engineering of anti-icing surfaces. Moreover, these insights shed light on the intricate mechanisms governing ice growth and melting, offering valuable guidance for the design and optimization of materials and surface coatings tailored to specific applications, ultimately contributing to advancements in technology, medicine, and environmental sustainability.

Finally, we mention that the introduction of additional variables such as ionic free energies [52–54], alongside modifications in pH or salt concentration, has the potential to shift the process from ice melting to ice formation. This emphasizes the need for future studies to consider these factors in predictive models to achieve a more comprehensive understanding of ice dynamics.

Ice growth and melting are inherently complex phenomena influenced by various forces. In addition to the dispersion forces (i.e., Casimir-Lifshitz interaction), ionic and electrostatic forces, as well as intrahydrogen bonding, also play crucial roles in determining the ice thickness. Past studies have accounted for impurity charges at the ice-water interface [2,3], and efforts have been made to improve theories of surface charging at these interfaces [53]. Recent work by Parsons *et al.* [55] has provided significant advances in understanding the role of ions and the autodissociation of water molecules at ice-water interfaces, emphasizing the importance of both structural forces [16,17] and Casimir-Lifshitz interactions. These findings suggest that salt forces, often previously misrepresented, are crucial in understanding ice premelting. Moving forward, predictive theories should integrate these effects to provide a more complete picture.

ACKNOWLEDGMENTS

The research contributions of O.I.M. and M.B. are part of the project No. 2022/47/P/ST3/01236 cofunded by the National Science Centre and the European Union's Horizon 2020 research and innovation programme under the Marie Skłodowska-Curie Grant Agreement No. 945339. Institutional and infrastructural support for the ENSEMBLE3 Centre of Excellence was provided through the ENSEMBLE3 project (MAB/2020/14) delivered within the Foundation for Polish Science International Research Agenda Programme and co-financed by the European Regional Development Fund and the Horizon 2020 Teaming for Excellence initiative (Grant Agreement No. 857543), as well as the Ministry of Education and Science initiative "Support for Centres of Excellence in Poland under Horizon 2020". S.K., B.G., and C.P. acknowledge also access to high-performance computing resources via NAISS, provided by NSC and PDC, as well as NOTUR, provided by Sigma2. V.E. acknowledges JDC2022-048530-I support funded by MICIU/AEI/10.13039/501100011033 and by the European Union (NextGenerationEU), the Ministerio de Universidades of Spain, and the University of Seville under the Grant Margarita Salas. M.B. gratefully acknowledges fruitful discussions with Dr. D. F. Parsons during the later stages of this work.

DATA AVAILABILITY

The data that support the findings of this study are available from the corresponding authors upon reasonable request.

[1] M. Elbaum and M. Schick, Application of the theory of dispersion forces to the surface melting of ice, Phys. Rev. Lett. **66**, 1713 (1991).

[2] L. A. Wilen, J. S. Wettlaufer, M. Elbaum, and M. Schick, Dispersion-force effects in interfacial premelting of ice, Phys. Rev. B **52**, 12426 (1995).

[3] J. S. Wettlaufer, Impurity effects in the premelting of ice, Phys. Rev. Lett. **82**, 2516 (1999).

[4] M. Elbaum, S. G. Lipson, and J. G. Dash, Optical study of surface melting on ice, J. Cryst. Growth **129**, 491 (1993).

[5] J. G. Dash, A. W. Rempel, and J. S. Wettlaufer, The physics of premelted ice and its geophysical consequences, Rev. Mod. Phys. **78**, 695 (2006).

[6] H. Li, M. Bier, J. Mars, H. Weiss, A.-C. Dippel, O. Gutowski, V. Honkimäki, and M. Mezger, Interfacial premelting of ice in nano composite materials, Phys. Chem. Chem. Phys. **21**, 3734 (2019).

[7] J. Benet, P. Llombart, E. Sanz, and L. G. MacDowell, Premelting-induced smoothening of the ice-vapor interface, Phys. Rev. Lett. **117**, 096101 (2016).

[8] J. Benet, P. Llombart, E. Sanz, and L. G. MacDowell, Structure and fluctuations of the premelted liquid film of ice at the triple point, Mol. Phys. **117**, 2846 (2019).

[9] D. N. Sibley, P. Llombart, E. G. Noya, A. J. Archer, and L. G. MacDowell, How ice grows from premelting films and water droplets, Nat. Commun. **12**, 239 (2021).

[10] M. B. Baker and J. G. Dash, Charge transfer in thunderstorms and the surface melting of ice, J. Cryst. Growth **97**, 770 (1989).

[11] J. G. Dash and J. S. Wettlaufer, The surface physics of ice in thunderstorms, Can. J. Phys. **81**, 201 (2003).

[12] S. C. Sherwood, V. T. J. Phillips, and J. S. Wettlaufer, Small ice crystals and the climatology of lightning, Geophys. Res. Lett. **33**, 2005GL025242 (2006).

[13] J. S. Wettlaufer, Surface phase transitions in ice: From fundamental interactions to applications, Philos. Trans. R. Soc. A **377**, 20180261 (2019).

[14] L. A. Wilen and J. G. Dash, Frost heave dynamics at a single crystal interface, Phys. Rev. Lett. **74**, 5076 (1995).

[15] J. Fiedler, M. Boström, C. Persson, I. H. Brevik, R. W. Corkery, S. Y. Buhmann, and D. F. Parsons, Full-spectrum high

resolution modeling of the dielectric function of water, J. Phys. Chem. B **124**, 3103 (2020).
[16] J. Luengo-Márquez and L. G. MacDowell, Lifshitz theory of wetting films at three phase coexistence: The case of ice nucleation on Silver Iodide (AgI), J. Colloid Interface Sci. **590**, 527 (2021).
[17] J. Luengo-Marquez, F. Izquierdo-Ruiz, and L. G. MacDowell, Intermolecular forces at ice and water interfaces: Premelting, surface freezing, and regelation, J. Chem. Phys. **157**, 044704 (2022).
[18] M. Boström, V. Esteso, J. Fiedler, I. Brevik, S. Y. Buhmann, C. Persson, S. Carretero-Palacios, D. F. Parsons, and R. W. Corkery, Self-preserving ice layers on CO_2 clathrate particles: Implications for enceladus, pluto and similar ocean worlds, Astron. Astrophys. **650**, A54 (2021).
[19] Y. Li, I. Brevik, O. I. Malyi, and M. Boström, Different pathways to anomalous stabilization of ice layers on methane hydrates, Phys. Rev. E **108**, 034801 (2023).
[20] A. Kobayashi, H. N. Golash, and J. L. Kirschvink, A first test of the hypothesis of biogenic magnetite-based heterogeneous ice-crystal nucleation in cryopreservation, Cryobiology **72**, 216 (2016).
[21] A. K. Kobayashi and T. D. Raub, Magnetite controls ice nucleation: Implications for cloud formation, in *AGU Fall Meeting Abstracts*, Vol. 2018 (American Geophysical Union, Washington, D.C., 2018), p. A14C-05.
[22] A. Kobayashi, M. Horikawa, J. L. Kirschvink, and H. N. Golash, Magnetic control of heterogeneous ice nucleation with nanophase magnetite: Biophysical and agricultural implications, Proc. Natl. Acad. Sci. **115**, 5383 (2018).
[23] V. Esteso, S. Carretero-Palacios, L. G. MacDowell, J. Fiedler, D. F. Parsons, F. Spallek, H. Míguez, C. Persson, S. Y. Buhmann, I. Brevik, and M. Boström, Premelting of ice adsorbed on a rock surface, Phys. Chem. Chem. Phys. **22**, 11362 (2020).
[24] Y. Li, K. A. Milton, I. Brevik, O. I. Malyi, P. Thiyam, C. Persson, D. F. Parsons, and M. Boström, Premelting and formation of ice due to Casimir-Lifshitz interactions: Impact of improved parameterization for materials, Phys. Rev. B **105**, 014203 (2022).
[25] I. E. Dzyaloshinskii, E. M. Lifshitz, and L. P. Pitaevskii, The general theory of van der Waals forces, Adv. Phys. **10**, 165 (1961).
[26] B. W. Ninham and V. A. Parsegian, van der Waals forces: Special characteristics in lipid-water systems and a general method of calculation based on the Lifshitz theory, Biophys. J. **10**, 646 (1970).
[27] P. Richmond and B. W. Ninham, Calculations, using Lifshitz theory, of the height vs. thickness for vertical liquid Helium films, Solid State Commun. **9**, 1045 (1971).
[28] P. Richmond and B. W. Ninham, A note on the extension of the Lifshitz theory of van der Waals forces to magnetic media, J. Phys. C **4**, 1988 (1971).
[29] G. H. Nyland and I. Brevik, van der Waals interaction between two cylinders in a magnetic fluid, Physica A **202**, 81 (1994).
[30] E. N. Velichko, G. L. Klimchitskaya, and E. K. Nepomnyashchaya, Casimir repulsion though a water-based ferrofluid, Mod. Phys. Lett. A **35**, 2040016 (2020).
[31] L. D. Landau, E. M. Lifshitz, and L. P. Pitaevskii, *Electrodynamics of Continuous Media*, 2nd ed., Course of Theoretical Physics, Vol. 8 (Butterworth-Heinemann, Oxford, 1998).
[32] G. Kresse and J. Hafner, *Ab initio* molecular dynamics for liquid metals, Phys. Rev. B **47**, 558 (1993).
[33] G. Kresse and D. Joubert, From ultrasoft pseudopotentials to the projector augmented-wave method, Phys. Rev. B **59**, 1758 (1999).
[34] J. P. Perdew, A. Ruzsinszky, G. I. Csonka, O. A. Vydrov, G. E. Scuseria, L. A. Constantin, X. Zhou, and K. Burke, Restoring the density-gradient expansion for exchange in solids and surfaces, Phys. Rev. Lett. **100**, 136406 (2008).
[35] S. L. Dudarev, G. A. Botton, S. Y. Savrasov, C. J. Humphreys, and A. P. Sutton, Electron-energy-loss spectra and the structural stability of nickel oxide: AnLSDA+U study, Phys. Rev. B **57**, 1505 (1998).
[36] I. Zorić, M. Zäch, B. Kasemo, and C. Langhammer, Gold, platinum, and aluminum nanodisk plasmons: Material independence, subradiance, and damping mechanisms, ACS Nano **5**, 2535 (2011).
[37] K. Jordan, A. Cazacu, G. Manai, S. F. Ceballos, S. Murphy, and I. V. Shevets, Scanning tunneling spectroscopy study of the electronic structure of Fe3O4 surfaces, Phys. Rev. B **74**, 085416 (2006).
[38] A. Hevroni, M. Bapna, S. Piotrowski, S. A. Majetich, and G. Markovich, Tracking the Verwey transition in single magnetite nanocrystals by variable-temperature scanning tunneling microscop, J. Phys. Chem. Lett. **7**, 1661 (2016).
[39] H. Liu and C. Di Valentin, Band gap in magnetite above Verwey temperature induced by symmetry breaking, J. Phys. Chem. C **121**, 25736 (2017).
[40] B. T. Draine and B. Hensley, Magnetic nanoparticles in the interstellar medium: Emission spectrum and polarization, Astrophys. J. **765**, 159 (2013).
[41] M. Boström, S. Kuthe, S. Carretero-Palacios, V. Esteso, Y. Li, I. Brevik, H. R. Gopidi, O. I. Malyi, B. Glaser, and C. Persson, Understanding ice and water film formation on soil particles by combining density functional theory and Casimir-Lifshitz forces, Phys. Rev. B **108**, 125434 (2023).
[42] M. Boström, M. R. Khan, H. R. Gopidi, I. Brevik, Y. Li, C. Persson, and O. I. Malyi, Tuning the Casimir-Lifshitz force with gapped metals, Phys. Rev. B **108**, 165306 (2023).
[43] Bo E. Sernelius, *Fundamentals of van der Waals and Casimir Interactions*, Springer Series on Atomic, Optical, and Plasma Physics (Springer International Publishing, New York, 2018).
[44] Y. Wang, S. R. Narayanan, and W. Wu, Field-assisted splitting of pure water based on deep-sub-Debye-length nanogap electrochemical cells, ACS Nano **11**, 8421 (2017).
[45] T.-H. Ou, B. Zhang, P. Hu, Z. Liu, Y. Wang, S. Hossain, S. Wang, S. Zhang, F. Liu, S. B Cronin *et al.*, Plasmon-enhanced sub-Debye-length nanogap photoelectrochemical cells for field-assisted electrolyte-free water splitting, J. Power Sources **617**, 235093 (2024).
[46] D. B. Hough and L. R. White, The calculation of Hamaker constants from Liftshitz theory with applications to wetting phenomena, Adv. Colloid Interface Sci. **14**, 3 (1980).
[47] M. Boström and Bo E. Sernelius, Thermal effects on the Casimir force in the 0.1−5 μm range, Phys. Rev. Lett. **84**, 4757 (2000).

[48] P. A. Maia Neto, F. S. S. Rosa, L. B. Pires, A. B. Moraes, A. Canaguier-Durand, R. Guérout, A. Lambrecht, and S. Reynaud, Scattering theory of the screened Casimir interaction in electrolytes, Eur. Phys. J. D **73**, 178 (2019).

[49] L. Ge, X. Shi, B. Li, and K. Gong, Fluctuation-induced dispersion forces on thin DNA films, Phys. Rev. E **107**, 064402 (2023).

[50] L. Ge, K. Liu, K. Gong, and R. Podgornik, Fabry-Pérot nanocavities controlled by Casimir forces in electrolyte solutions, Phys. Rev. Appl. **21**, 044040 (2024).

[51] L. B. Pires, D. S. Ether, B. Spreng, G. R. S. Araújo, R. S. Decca, R. S. Dutra, M. Borges, F. S. S. Rosa, G.-L. Ingold, M. J. B. Moura, S. Frases, B. Pontes, H. M. Nussenzveig, S. Reynaud, N. B. Viana, and P. A. Maia Neto, Probing the screening of the Casimir interaction with optical tweezers, Phys. Rev. Res. **3**, 033037 (2021).

[52] D. F. Parsons and A. Salis, The impact of the competitive adsorption of ions at surface sites on surface free energies and surface forces, J. Chem. Phys. **142**, 134707 (2015).

[53] P. Thiyam, J. Fiedler, S. Y. Buhmann, C. Persson, I. Brevik, M. Boström, and D. F. Parsons, Ice particles sink below the water surface due to a balance of salt, van der Waals, and buoyancy forces, J. Phys. Chem. C **122**, 15311 (2018).

[54] D. F. Parsons and A. Salis, A thermodynamic correction to the theory of competitive chemisorption of ions at surface sites with nonelectrostatic physisorption, J. Chem. Phys. **151**, 024701 (2019).

[55] D. F. Parsons, P. Thiyam, and M. Boström (private communication).

Correction: Funding statements in the Acknowledgment section were incorrect and have been fixed.